An Adaptive Impedance-Matching System for Vehicular Power Line Communication

Nima Taherinejad, *Member, IEEE*, Lutz Lampe, *Senior Member, IEEE*, and Shahriar Mirabbasi, *Member, IEEE*

***Abstract*—Vehicular power line communication (VPLC) is being considered as a potential solution to mitigate the increase of complexity and cost of the automotive wiring harness caused by the growth of the number of electronic devices and sensors deployed inside vehicles. This is because VPLC reuses power cables for data communication and, thus, avoids the need for additional communication wires. However, this reuse does not come without problems. One of the challenges for VPLC is the time, frequency, and location dependence of the access impedance, which can cause severe impedance mismatch for the communication signal. Impedance mismatch degrades the signal-to-noise-power ratio at the communication receiver and thus affects transmission reliability. Due to the variable nature of the access impedance, a fixed matching circuit will be inefficient. Hence, in this work, we present an *adaptive* impedance-matching system, which improves the communication-signal transfer from the transmitting to the receiving device. The system is evaluated via simulations for a wide range of access-impedance test points and S-parameters of VPLC networks obtained in previous measurement campaigns. Our simulation results demonstrate that the presented adaptive matching system is able to achieve VPLC signal-power transfer within 30% of the theoretical optimum. This translates to a power gain, up to a factor of 10, which is larger than that of other solutions reported in the literature.**

***Index Terms*—Access impedance, adaptive impedance matching, impedance mismatch, vehicular power line communication (VPLC).**

I. Introduction

THE use of power lines for communication purposes is a concept dating back to the early 1900s [1]. It has widely been applied for power-grid monitoring and control, including smart meter reading, home and industry automation, and in-home multimedia communication [2], [3]. The significant growth of the number of electronic devices and sensors in vehicles [4]–[6], which is further spurred by the increasing role of electric vehicles in the automotive market, has stimulated interest, research, and development activities in the field of vehicular power line communication (VPLC) [7]–[18]. Since VPLC reuses power cables and thus avoids the need for installing additional wires dedicated for data communication, it is considered as a means to reduce cost and complexity of the vehicle wiring harness. On the negative side, VPLC is affected by transmission channel imperfections, which includes impulsive noise [15], [19], frequency selectivity of the channel transfer function [12], [14], [16]–[18], and time- and location-dependent network access impedance [20], [21]. The latter causes a general impedance mismatch for VPLC transmitters and receivers, which results in suboptimal signal coupling from the transmitter to the network and from the network to the receiver, which in turn weakens the power line communication (PLC) signal transfer. While channel frequency-selectivity and noise can be addressed through the design of appropriate transmission formats and signal processing, impedance mismatch requires the use of impedance-matching circuits at VPLC transmitters and receivers. However, conventional matching circuits using fixed passive elements are not effective due to the variability of the access impedance with time and location, which is caused by time-varying network loads and signal reflections in the power line.

In this paper, we present and evaluate an adaptive impedance-matching design that can adjust the matching circuits for each instance of access impedance, as monitored by its sensing unit. Preliminary results of our design were presented in [1] and [2]. We consider matching both at the transmitter side for signal coupling and at the receiver side for signal decoupling, and we discuss the simultaneous operation of transmitter- and receiver-side impedance matching. To demonstrate the merit of our design, we use the data obtained in our measurement campaigns [16], [21] and test the system for a wide range of access-impedance values. The bandwidth of the matching circuit is also simulated, and other important issues such as adaptation delay are discussed.

To put our impedance-matching design into context, we continue the discussion with a brief classification of matching approaches and a literature review in the next section. Then, we present our approach to the matching problem in Section III. Section IV describes the design process and the details of each unit in the system. Extensive simulation results are presented and discussed in Section V. Finally, the paper is concluded in Section VI.

II. Classification of Impedance Matching Systems and Literature Review

The design of coupling circuitry has been studied since the first uses of PLC [4, Ch. 4]. Since VPLC operates over DC

Manuscript received March 2, 2016; accepted April 20, 2016. Date of publication May 4, 2016; date of current version February 10, 2017. This work was supported in part by the AUTO21 Network of Centres of Excellence, the Natural Sciences and Engineering Research Council of Canada, and by the Partners for the Advancement of Collaborative Engineering Education Program. Parts of this work were published at the IEEE International Symposium of Power Line Communication and Its Applications (ISPLC) in 2012 and 2014. The review of this paper was coordinated by Prof. L. Guo.

N. Taherinejad was with the Department of Electrical and Computer Engineering, The University of British Columbia, Vancouver, BC V6T 1Z4, Canada. He is now with the TU Wien, 1040 Vienna, Austria (e-mail: nima.taherinejad@tuwien.ac.at).

L. Lampe and S. Mirabbasi are with the Department of Electrical and Computer Engineering, The University of British Columbia, Vancouver, BC V6T 1Z4, Canada (e-mail: lampe@ece.ubc.ca; shahriar@ece.ubc.ca).

Color versions of one or more of the figures in this paper are available online at http://ieeexplore.ieee.org.

Digital Object Identifier 10.1109/TVT.2016.2562629

TABLE I
CLASSIFICATION OF IMPEDANCE-MATCHING SOLUTIONS

Criterion	Classes	Brief Description
Method	Numerical	Real Frequency Technique
	Analytical	Circuit models
Load/Source Impedance Type	Double	Complex/Complex
	Single	Complex/Resistive
	Insertion Loss	Resistive/Resistive
Structure	Fixed	One circuit topology
	Flexible	Changing topologies
Implementation	Passive	On-chip, off-chip (bulky)
	Active	Easily integrated
Bandwidth	Narrowband	
	Wideband	

TABLE II
COMPARING CURRENT WORK TO OTHER RELATED WORKS

Work	[27]	[20]	[28]	[29]
Methodology	Analytical	Analytical	Numerical	Analytical
Impedance Type	Insertion Loss	Single	Single	Single
Structure	Fixed	Fixed	Flexible	Flexible
Implementation	Passive	Combination	Passive	Combination
Bandwidth	Narrow	Narrow	Wide	Narrow
Notes	Bulky, heavy and expensive transformers	Transformers used, alleviated method	Complex control system (M-PSO)	Control system not discussed

power systems, theoretically, a single capacitor could be used to couple and decouple the high-frequency communication signal. However, this would be suboptimal, considering the communication-signal transfer. To address this issue, a coupling circuit is necessary that is able to match the impedance between the network and the VPLC modems. Here, we first briefly introduce the general concept of impedance matching and then review some of the PLC matching systems presented in the literature.

A. Impedance Matching: Concept and Classification

Considering a power source with an internal impedance connected to a load and writing the respective circuit solution, it can be easily derived that maximum power is transferred to the load if the load impedance is equal to the complex conjugate of the source internal impedance. In the context of VPLC, at the transmitter, the load is the vehicle harness. Its Thévenin/Norton equivalent impedance, i.e., the access impedance, is considered as the load impedance, and this should be complex-conjugate matched to the transmitter's internal impedance. At the receiver side, the load is the receiver's input impedance, which should be complex-conjugate matched to the harness access impedance as observed from the receiver side. Using fixed VPLC transmitter and receiver impedances, e.g., 50 Ω, will most often result in impedance mismatch, since the access impedance is dependent on the point of coupling/decoupling and varies with time. Therefore, to maximize signal-power transmission into the network at the transmitter side and out of the network at the receiver side, adaptive impedance-matching circuits are needed. To match the impedance without any power loss, lossless passive elements need to be used (cf., e.g., [22], [23, Ch. 5], [24], and [25]).

Table I shows a classification of impedance-matching solutions, according to the criterion shown in the first column. Numerical methods use mathematics (nonlinear optimization simulator in the case of Real Frequency Technique [26] example) for finding an optimum matching solution over a given range of frequency, whereas to this end, analytical methods use circuit models for the channel and devices in the design. In terms of source and load impedance, the matching could be done for impedances of resistive to resistive (Insertion Loss), resistive to complex (Single Matching), or complex to complex (Double Matching) nature. The structure (topology of the circuit) could be fixed or flexible, where in the latter case, the circuit topology changes based on the needs. Matching circuits can be implemented using passive elements (RLC) or active elements (such as active inductors and operational amplifiers), and the objective could be matching over a relatively narrow or wide bandwidth. See [1] for more details on each class. All the classes could potentially be used in an appropriate setup to address a matching problem. The remainder of this section is dedicated to a review of adaptive impedance-matching systems, specifically those which were designed for PLC applications. Table II presents a summary of these works and how they fit into classes from Table I. The distinguishing features of these works are briefly reviewed in Section II-B, and we invite the reader to consult [1] for a longer review or the given reference of each work for full details.

B. Related Works

In earlier approaches such as the one by Mavretic *et al.* [27], PLC systems were designed mostly with a focus on resistive loads and sources (insertion loss problem). Use of bulky, heavy, and expensive transformers was also a common practice. To address this issue, Park *et al.* [20] use a voltage-controlled general impedance converter, as proposed in [30], to build active inductors in a more compact way as opposed to passive inductors. One of the limiting factors for active inductors, however, is the maximum current and voltage supported by operational amplifiers used in the circuit. They try to solve this problem with the addition of a fixed passive inductor and a transformer, which would be smaller, considering the simultaneous use of the active inductor. However, by using a transformer and an off-chip inductor, they forfeit part of the advantages gained from applying an active inductor.

Some efforts were also turned toward wideband impedance-matching systems. For example, Araneo *et al.* [28] use an LC-ladder structure and a numerical method to fit the structure parameters. Numerical optimization is accomplished with a meta-particle swarm optimization (M-PSO) algorithm. As illustrated in Fig. 1 (results taken from [28]), this method can achieve an improved power transmission over a relatively wide frequency range. However, using a numerical method requires a digital processor capable of solving the optimization problems fast enough to provide the solution within a reasonable delay time. Aiming at inexpensive and small-area integrated solutions, this can be considered as a disadvantage.

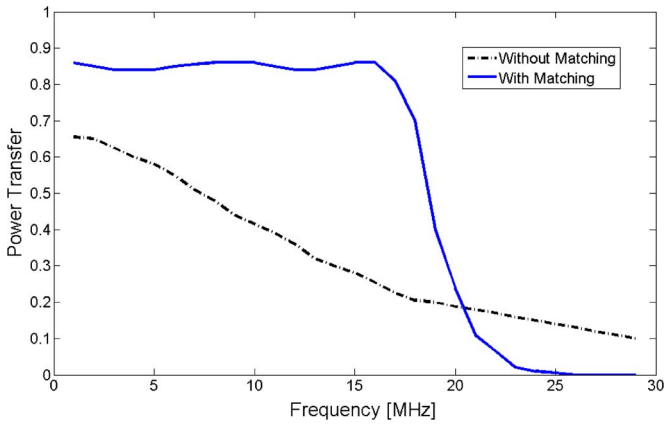

Fig. 1. Power transfer between modem and power line with (blue solid line) and without (black dashed line) Araneo's wideband impedance matching. Results taken from [28, Fig. 5].

Finally, our approach for narrowband matching, which was first proposed in [1], was adopted by Nisbet *et al.* in [29]. The capability of transformerless impedance matching (at the transmitter side) is demonstrated for a range of access impedances. However, it is not entirely clear in what way the design extends beyond [1], as the control and some other parts of the system, which have a major impact on the performance, are not explained.

In the following, we build on our previous work in [1] and [2], enhance the design for transmitter-side matching, and propose a new design for receiver-side matching. We will then elaborate on the details of the control system. Finally, we present simulations for our impedance-matching solutions and demonstrate the suitability of the design even for wideband applications.

III. Our Approach to the Matching Problem

Here, we first introduce our approach to solve the matching problem at one end of the communication system. At the transmitter side, the source and its internal impedance interact with the network, which is represented by its equivalent impedance, i.e., the access impedance. On the receiver side, the network is represented with its Thévenin equivalent circuit and interacts with the receiver's input impedance. Then, we will explain that, based on the results from our previous measurement campaigns, matching at one side of the network does not have a significant impact on matching at the other side in VPLC. Hence, independent matching at the transmitter and the receiver will be a practically meaningful solution for the matching problem in VPLC applications.

A. Impedance Matching at One End

There are several ways to approach the matching problem. A useful tool that aids the understanding of the underlying concepts is the Smith chart. The Smith chart efficiently visualizes the location of impedances and the effect of adding various impedances to a network. Therefore, in the following, we will use the Smith chart to facilitate the understanding of the derivation of our impedance-matching system. We would like to emphasize, however, that the Smith chart is not part of the actual impedance-matching implementation.

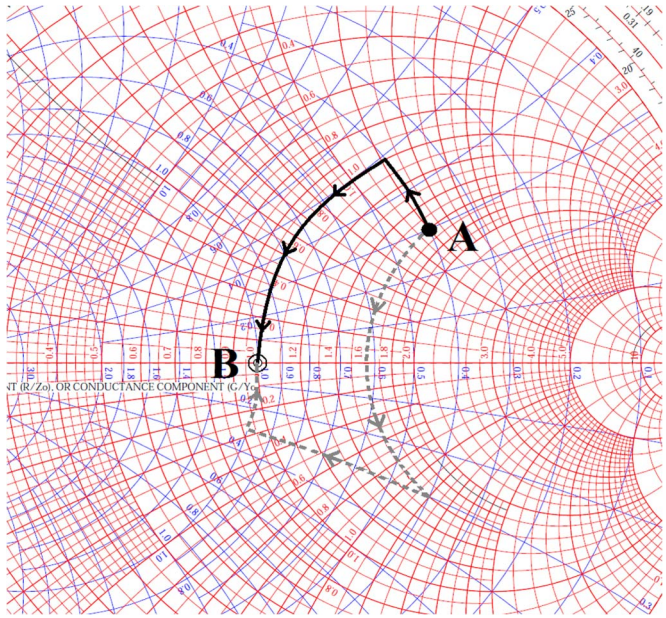

Fig. 2. Matching problem demonstrated in the Smith chart. From a given impedance, i.e., point A, to the desired impedance, i.e., point B, there are several paths (two samples shown), which could be implemented through matching circuits.

The matching problem is finding a circuit that changes an impedance observed at one of its ports to another impedance at the other port. In the Smith chart, this circuit can be represented as a path going from a point A, i.e., the original impedance, to the desired point B, i.e., the matched impedance. The latter is often at the center of the Smith chart. Fig. 2 shows two different sample paths from point A to point B. One can find many other paths connecting these two points. However, a lossless solution can be obtained by only traversing constant conductance or constant resistance contours. This consideration reduces the number of possible paths, but there are still many options. Another limiting factor to be considered can be the number of moves along these contours. Since each move represents a series or parallel non-resistive element in the matching circuit, more moves entail the use of more components and consequently result in a more complex circuit structure. This also imposes an extra burden to the control logic for adaptation. Therefore, matching with fewer moves (e.g., two for the black solid line in Fig. 2) is preferred over matching with more moves (e.g., three for the gray dotted line in Fig. 2).

Following the aforementioned rationale, we adopt a two-move strategy to perform the matching. The first move is along a constant conductance contour to reach the constant resistance contour of the matching target, or along a constant resistance contour to reach the constant conductance contour of the matching target. This compensates for the real part of the impedance mismatch. The second move is along the constant resistance or conductance contour until the matching target is reached, and it thus compensates for the imaginary part of the mismatch. Constant conductance moves are accomplished through a

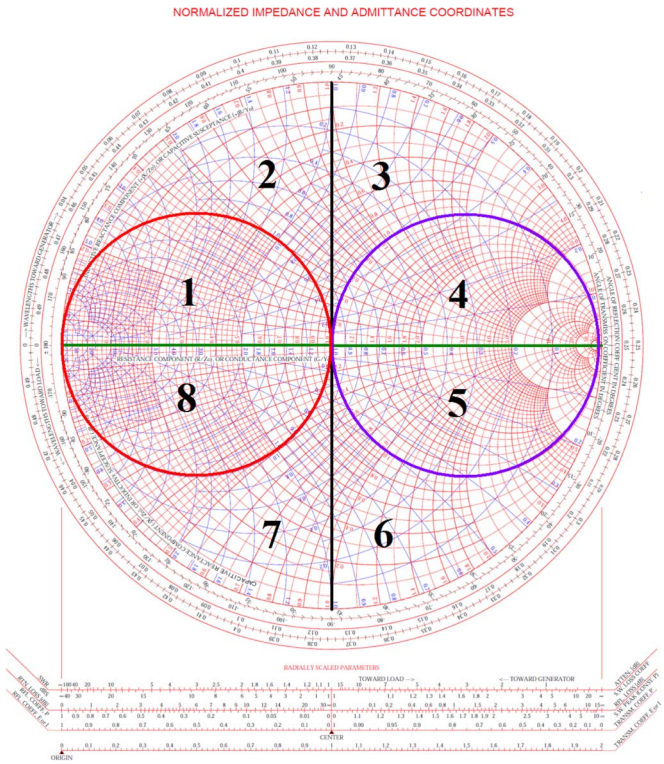

Fig. 3. Smith chart divided into eight regions to categorize different movements.

parallel inductor or capacitor, and constant resistance moves are achieved with a series inductor or capacitor.

Normalizing the Smith chart with the target impedance,[1] so that it is represented by the center point of the chart, Fig. 3 shows the perfect-match conductance and resistance circles in red and purple, respectively. Therefore, our first move from any point is to reach one of these circles. To choose the path to these circles, the location of the original impedance point in the Smith chart is important, since it determines the type of element used for achieving this move. It matters whether the original impedance value is inside or outside one of the circles and whether it is above or below the green line shown in Fig. 3 (for a resistive target impedance, above and below the green line means inductive and capacitive original impedances, respectively). Furthermore, for the regions outside the circles, the moves are determined by which of the two circles is closer. Hence, the Smith chart is divided into the eight regions shown in Fig. 3.

For transmitter-side impedance matching, we move from the network access impedance (the original impedance) to the internal impedance of the modem (i.e., the target impedance, which is obtained from the modem specification). Depending on the region of the Smith chart into which the access impedance falls, we apply the combination of elements in the matching circuit shown in the left part of Table III. These combinations will bring us to the center of the Smith chart. To reuse the same circuitry for receiver-side matching, the original and the target impedance change their roles, and we need to move from the center of the Smith chart (corresponding to the known impedance of the receiving modem, which is again a given parameter in the modem specification) to the access-impedance point in the Smith chart. This is accomplished by traversing the paths from transmitter-side matching in reverse direction, for which the circuit-element combinations are shown in the rightmost part of Table III. We will apply the insights gained from the Smith chart analysis when designing the impedance matching and control units in Section IV.

[1]The target impedance is the modem impedance for our application, and it is assumed to be a given design parameter. This information can be obtained from the modem specifications, which includes its input and output equivalent Thévenin/Norton models.

B. Impedance Matching at Both Ends

The VPLC network access impedance is clearly dependent on the loads connected to the power harness, which makes it dependent on the state of these loads and, thus, time varying. Measurement results in, for example, [14, Fig. 8] and [21, Figs. 5 and 6] show such dependencies as a function of the vehicle ignition state. This means that, strictly speaking, transmitter- and receiver-side matching should be performed jointly. However, it is interesting to look at the effect of changing the load impedance at one end (via impedance matching) onto the access impedance at the other end of the communication link.

To this end, we consider S-parameter channel data obtained in our measurement campaigns reported in [16] and [21]. In particular, we compute the reflection coefficients [23]

$$\Gamma_{\text{in}} = S_{11} + \frac{S_{12}S_{21}}{1 - S_{22}\Gamma_L}\Gamma_L \tag{1}$$

at the transmitter side of the network, as a function of the reflection coefficient of the load impedance Γ_L, and

$$\Gamma_{\text{out}} = S_{22} + \frac{S_{12}S_{21}}{1 - S_{22}\Gamma_S}\Gamma_S \tag{2}$$

at the receiver side of the network, as a function of the source reflection coefficient Γ_S. S_{ij} are the measured S-parameters, and the relationship between a reflection coefficient Γ and an impedance Z is given by

$$\Gamma = \frac{(Z - Z_0)}{(Z + Z_0)} \tag{3}$$

where the reference impedance $Z_0 = 50\ \Omega$ for our measurements [16], [21]. For the following, we choose Γ_L and Γ_S corresponding to the six impedance values $\{0.1, 1, 10, 50, 100, 250\}\ \Omega$, which cover the whole range for the real part of access impedances that we have observed in our measurement campaigns. In addition, we consider the case of perfect impedance matching, for which [31]

$$\Gamma_S = \frac{B \pm \sqrt{B^2 - 4|C|^2}}{2C} \tag{4}$$

where

$$\begin{aligned} B &= 1 + |S_{11}|^2 - |S_{22}|^2 - |S_{11}S_{22} - S_{21}S_{12}|^2 \\ C &= S_{11} - S_{22}^*|S_{11}S_{22} - S_{21}S_{12}| \end{aligned} \tag{5}$$

and Γ_L has the same form as (4) with S_{11} and S_{22} swapped in (5).

TABLE III
COMBINATION OF ELEMENTS IN THE MATCHING CIRCUIT TO ACHIEVE MATCHING IF NETWORK ACCESS IMPEDANCE IS IN DIFFERENT REGIONS SHOWN IN FIG. 2

	Transmitter-side matching	**Receiver-side matching**
Region	Combination	Combination
1	series inductor followed by a parallel capacitor	parallel inductor followed by series capacitor
2	series capacitor followed by a parallel capacitor	parallel inductor followed by a series inductor
3	parallel capacitor followed by a series capacitor	series inductor followed by a parallel inductor
4	parallel inductor followed by a series capacitor	series inductor followed by a parallel capacitor
5	parallel capacitor followed by a series inductor	series capacitor followed by a parallel inductor
6	parallel inductor followed by a series inductor	series capacitor followed by a parallel capacitor
7	series inductor followed by a parallel inductor	parallel capacitor followed by a series capacitor
8	series capacitor followed by a parallel inductor	parallel capacitor followed by a series inductor

TABLE IV
EFFECT OF TERMINATION AT ONE END OF A VPLC LINK ON THE OTHER END FOR SEVERAL MEASURED LINKS. AVERAGE (AVG) AND MAXIMUM (MAX) CHANGES FOR SEVEN TERMINATION IMPEDANCES

Link (from [16], [21])	Effect on $\Gamma_{\rm in}$ (%)		Effect on $\Gamma_{\rm out}$ (%)	
	Avg	Max	Avg	Max
VCU-DMOC	0.08	1.41	0.09	2.11
VCU-DC/DC	0.005	0.67	0.002	0.13
DC/DC-DMOC	0.01	0.11	0.03	0.71
HVBat-DMOC	0.42	6.61	0.19	4.58
Average/Max for [16]	*0.13*	*6.61*	*0.08*	*4.58*
Bat-Cigar	0.05	1.25	0.11	1.13
Bat-Trunk	0.08	3.44	0.18	12.44
Bat-Tail-R	0.02	0.61	0.05	3.56
Bat-Front-L	0.07	1.80	0.20	3.74
Average/Max for [21]	*0.06*	*3.44*	*0.14*	*12.44*
Total Average/Max	**0.10**	**6.61**	**0.11**	**12.44**

The effect of varying the termination impedance at one side of the VPLC link according to the seven cases specified earlier is shown in Table IV. We consider four links of a hybrid-electric vehicle measured in [16] and four links of a combustion-engine vehicle measured in [21], respectively, and the results are the average and maximal deviations for the seven scenarios over the frequency range from 100 kHz to 100 MHz. We observe that the effect of changing the load at one end of the link onto the other end is overall fairly moderate. Even the maximal change is only in one case more than 10%, which is due to deep notches observed in the channel transfer function. These results suggest that performing impedance matching independently at the transmitter and the receiver side should not incur notable performance penalties compared to joint matching at both ends of the link. Since the latter would require the exchange of access-impedance measurements, we prefer and pursue the independent matching approach in the following.

IV. SYSTEM DESIGN

Having established the basic principles of our approach to impedance matching, here, we explain the details of our matching system.

A. Basic Structure and Operation

The block diagram of the proposed adaptive impedance-matching system is shown in Fig. 4. It is implemented at the transmitter and receiver side, and each system consists of three main units: measurement unit, impedance-matching unit, and control unit. To enable the matching, we assume that the communication device sends a tone at a frequency of f_c, which is the center frequency for the band in which matching is to be achieved. When the measurement unit is settled, the control unit adjusts the matching circuit elements in the matching unit. The adjustment at a considered device can be different, depending on whether transmitter-side or receiver-side matching is performed. Hence, a device could have two different matching units, i.e., one for transmission and one for reception, or the same matching unit can be used but its setting would change from transmission to reception. After setting the values in the matching unit, devices go to their normal state of transmission or reception of data. Adaptation of the matching circuit can be done periodically or on demand when transmitting or receiving data.

B. Measurement Unit

The measurement unit senses physical parameters and provides this information to the control unit for decision making. Fig. 5 shows the structure of the measurement unit, which can be divided into the sensing unit and the interpretation unit.

The details of the sensing unit are shown in Fig. 6. A very small resistor (e.g., 0.1–1 Ω) is used for sensing, and two operational amplifiers (Op-Amps) amplify the sensed signals. One Op-Amp measures the voltage across the resistor, from which the current going through it, i.e., I_s is obtained. The other Op-Amp measures the voltage between the input node and the reference node (ground), i.e., V_s. Given the single-tone signal, we have

$$V_s(t) = \sqrt{2} V_{\rm env} \cos(2\pi f_c t + \phi) \tag{6}$$

$$I_s(t) = \sqrt{2} I_{\rm env} \cos(2\pi f_c t). \tag{7}$$

The interpretation unit is supplied with the voltage and current signals generated by the sensing unit and outputs four control signals, i.e., $V_{\rm env}$, $I_{\rm env}$, $P_{\rm act}$, and $B_{\rm sign}$, that are used by the control unit (see Fig. 4). $V_{\rm env}$ and $I_{\rm env}$ are the envelope values of the measured voltage and current signals in (6) and (7), respectively, and generated by the circuit shown in Fig. 7. Multiplying V_s and I_s gives the instantaneous source power

$$\begin{aligned} P_s(t) &= 2K V_{\rm env} I_{\rm env} \cos(2\pi f_c t + \phi) \cos(2\pi f_c t) \\ &= K V_{\rm env} I_{\rm env} \left[\cos\left(2\pi (2f_c) t + \phi\right) + \cos(\phi)\right] \end{aligned} \tag{8}$$

where K is a constant denoting the overall gain of the multiplier circuit. This is followed by low-pass filtering, which provides the active-power measurement ("$*$" denotes convolution)

$$P_{\rm act}(t) = (h_{\rm LP} * P_s)(t) \tag{9}$$

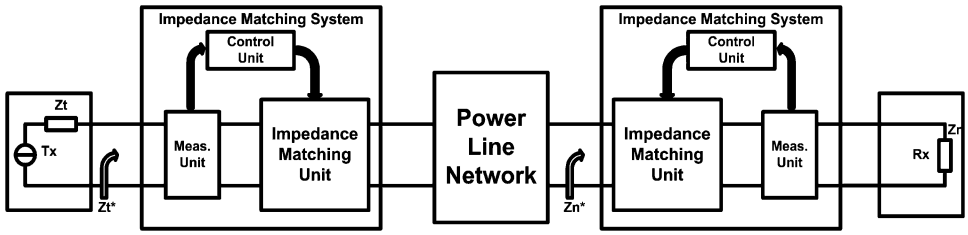

Fig. 4. Block diagram of the proposed adaptive impedance-matching system for the transmitter and receiver side. Z_t and Z_n denote the source impedance at the transmitter and network access impedance observed from the receiver, respectively. Z_t^* and Z_n^* indicate the *desired* impedance matching at the transmitter and receiver, respectively.

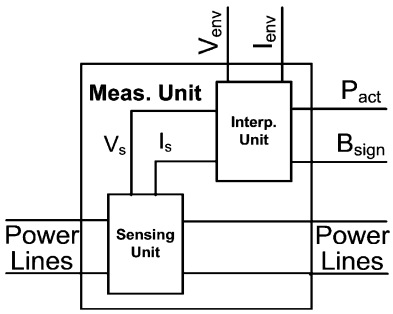

Fig. 5. Block diagram of the measurement unit.

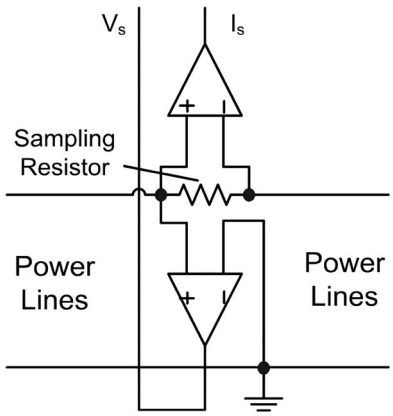

Fig. 6. Circuit-level block diagram of the sensing unit.

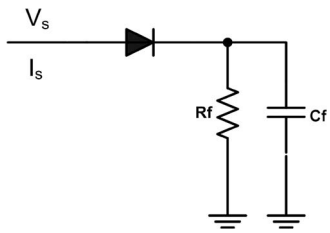

Fig. 7. Envelope detecting circuit used in the interpretation unit. In this paper, the values were selected as $R_f = 1$ kΩ and $C_f = 1.4$ pF.

which converges to $KV_{\rm env}I_{\rm env}\cos(\phi)$. The circuit-level block diagram for the active-power measurement is shown in Fig. 8. Finally, $B_{\rm sign}$ is a Boolean variable that indicates whether a load is inductive ($B_{\rm sign} = 0$) or capacitive ($B_{\rm sign} = 1$). The circuit shown in Fig. 9 generates $B_{\rm sign}$ by comparing the values of voltage and current at the zero crossings.

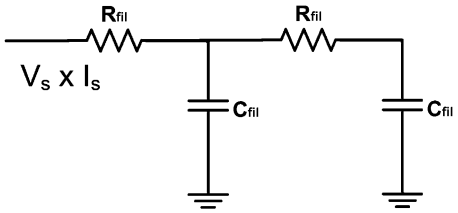

Fig. 8. Second-order low-pass RC filter for active-power measurement $P_{\rm act}$. Used values were selected as $R_{\rm fil} = 10$ kΩ and $C_{\rm fil} = 6$ pF.

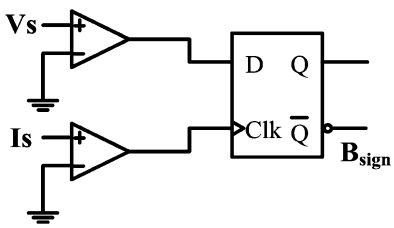

Fig. 9. Circuit used to discern capacitive versus inductive loads based on zero crossings. The output is "1" if the load is capacitive and "0" if inductive.

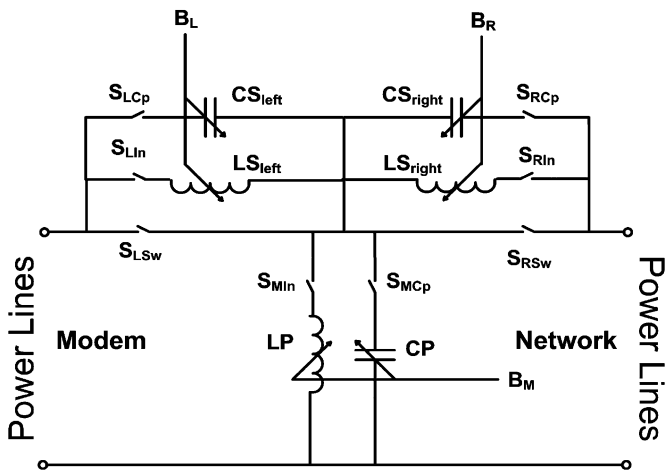

Fig. 10. Circuit structure of the matching unit (see Fig. 4).

C. Matching Unit

As explained in Section III-A, an arrangement of L-structured inductors and/or capacitors can perform the impedance matching, leading to the maximum active-power transfer between the modem and the network. Fig. 10 shows the corresponding circuit structure that can be used for this impedance matching.

This unit turns the bias voltages B_L, B_R, and B_M into the actual capacitance and inductance values according to

$$\text{LP} = \frac{Z_0}{2\pi f_c V_B} \tag{10}$$

$$\text{CP} = \frac{V_B}{2\pi f_c Z_0} \tag{11}$$

$$\text{LS} = \frac{V_B Z_0}{2\pi f_c} \tag{12}$$

$$\text{CS} = \frac{V_B Z_0}{2\pi f_c} \tag{13}$$

where V_B is to be substituted by B_L, B_R, and B_M according to Fig. 10 and $Z_0 = 50\ \Omega$. The bias voltages and switches shown in Fig. 10 are adjusted by the control unit described next.

D. Control Unit

The control unit (see Fig. 4) uses the input from the measurement unit to provide the matching unit with control signals that determine the state of the switches, as well as the normalized values of the components in the matching circuit shown in Fig. 10. This is done by determining the access impedance's value and comparing it to the target impedance. On the Smith chart, this would correspond to finding the position of the access impedance with respect to the eight different regions in Fig. 3.

To this end, first, the measured impedances are identified as inductive or capacitive (above or below the green line in Fig. 3) using the B_{sign} signal provided by the measurement unit. Next, we determine whether $V_{\text{env}}/I_{\text{env}}$ is smaller or larger than the modem impedance. In the Smith chart representation, this would be whether the impedance is in the left- or right-hand side half of the Smith chart, i.e., left or right of the black line in Fig. 3. Writing the real and imaginary parts of the reflection coefficient $\Gamma = a + jb$, we have

$$\begin{aligned} Z &= Z_0 \frac{1+\Gamma}{1-\Gamma} = Z_0 \frac{1+a+jb}{1-a-jb} \\ &\Rightarrow |Z| = \frac{V_{\text{env}}}{I_{\text{env}}} = |Z_0| \frac{(1+a)^2+b^2}{(1-a)^2+b^2} \\ &\Rightarrow \frac{V_{\text{env}}}{I_{\text{env}}} \lessgtr |Z_0| \Leftrightarrow \frac{(1+a)^2+b^2}{(1-a)^2+b^2} \lessgtr 1 \\ &\Leftrightarrow a \lessgtr 0 \end{aligned} \tag{14}$$

where the reference impedance Z_0 is the impedance of the transmitter/receiver-modem for transmitter/receiver-side matching. Hence, if $V_{\text{env}}/I_{\text{env}}$ is smaller than the modem impedance, then the measured access impedance is located on the left half of the Smith chart and *vice versa*.

Finally, we need to determine whether the real part of impedance or admittance is smaller than that of the target impedance or admittance or not. On the Smith chart, this corresponds to whether the impedance lies inside or outside the perfect-match circles shown in Fig. 3. Starting with the right circle, it can be observed that all the impedances inside have real parts that are larger than that of the modem impedance. Similarly, admittance values inside the left circle have real parts that are bigger than that of the modem admittance. We obtain these real parts from the measured quantities as

$$Z_r = \frac{P_{\text{act}}}{I_{\text{env}}^2} \tag{15}$$

$$Y_r = \frac{P_{\text{act}}}{V_{\text{env}}^2} \tag{16}$$

and compare them to the real parts of the modem impedance and admittance, i.e., $Z_{r,0}$ and $Y_{r,0}$. That is, we compare the normalized quantities $Z_r' = Z_r/Z_{r,0}$ and $Y_r' = Y_r/Y_{r,0}$ to one.

Table V summarizes how we determine the location of the impedance in the Smith chart. This provides the control unit with all the necessary information regarding the type of moves and their respective order, directions, and signs. Together with the matching steps described in Table III, this leads to the logic for the switches in the matching unit in Fig. 10 shown in Table VI for the transmitter and the receiver side. The bit stream from most significant bit (MSB) to the least significant bit (LSB) shows the status of each switch in the following order: S_{LSw}, S_{LIn}, S_{LCp}, S_{MIn}, S_{MCp}, S_{RIn}, S_{RCp}, S_{RSw}.

The values for the capacitor and inductor elements are also decided by the control unit. To find a relation between inputs, i.e., measured parameters, and assigned values for each element of the matching circuit, the magnitudes of the phase changes

TABLE V
LOGIC TO DETERMINE LOCATION OF IMPEDANCE IN THE SMITH CHART BASED ON MEASURED VARIABLES

B_{sign}	$(V_{\text{env}}/I_{\text{env}})/Z_0$	Z_{r}', Y_{r}'	Region
'1'	≥ 1	$Z_{\text{r}}' \geq 1$	5
		$Z_{\text{r}}' < 1$	6
	< 1	$Y_{\text{r}}' \geq 1$	8
		$Y_{\text{r}}' < 1$	7
'0'	≥ 1	$Z_{\text{r}}' \geq 1$	4
		$Z_{\text{r}}' < 1$	3
	< 1	$Y_{\text{r}}' \geq 1$	1
		$Y_{\text{r}}' < 1$	2

TABLE VI
LOGIC TABLE FOR SWITCHES IN THE MATCHING UNIT OF THE TRANSMITTER AND THE RECEIVER SIDE. THE BIT STREAM REPRESENTS THE STATUS OF SWITCHES IN THE FOLLOWING ORDER FROM MSB TO LSB: S_{LSw}, S_{LIn}, S_{LCp}, S_{MIn}, S_{MCp}, S_{RIn}, S_{RCp}, S_{RSw}. "0" REPRESENTS THE OPEN-CIRCUIT STATE OF THE SWITCH, "1" IS THE SHORT-CIRCUIT STATE, AND "X" MEANS THE DON'T CARE STATE

Region	Switches at Tx	Switches at Rx
1	"1XX01100"	"00110XX1"
2	"1XX01010"	"01010XX1"
3	"01001XX1"	"1XX10100"
4	"00110XX1"	"1XX01100"
5	"01001XX1"	"1XX10010"
6	"01010XX1"	"1XX01010"
7	"1XX10100"	"00101XX1"
8	"1XX10010"	"01001XX1"

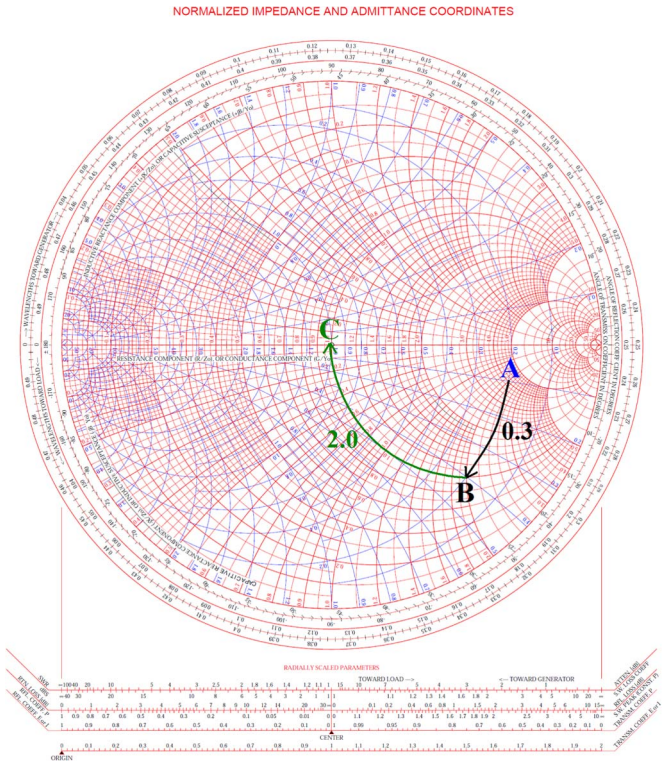

Fig. 11. Matching an impedance at point A in the Smith chart.

(i.e., lengths of moves in the Smith chart) need to be determined. For transmitter-side matching, this means that, first, the magnitude of the phase change that is necessary to compensate for the real part (to arrive at the respective perfect-match circle of resistance or conductance) is estimated. Then, the magnitude of the phase change to move from this new point to the target impedance (traversing on the perfect-match circle to the center, i.e., the perfect match point) is determined. For receiver-side matching, the calculation are the same, but in reverse order, as the matching unit needs to move first from the center toward the target impedance on the perfect-match circle and then to the location of the access impedance.

To be specific on how we estimate the lengths of the moves, let us assume that, for the transmitter side, we aim to match an access impedance located at point A in the right-hand side of the Smith chart, as shown in Fig. 11. The first move needs to change the susceptance from -0.1 at A to -0.4 at point B on the perfect-match circle. We approximate the relation between the susceptance y of the target point B and the normalized conductance $x = Y_r'$ of the access-impedance point A by the second-order polynomial expression

$$y = 0.01 + 2.15x - 2.15x^2. \tag{17}$$

The magnitude of susceptance change needed for the first move is thus calculated as

$$\Delta_{\text{mov1}} = |Y_i' - y| \tag{18}$$

where $Y_i' = \sqrt{|Y'|^2 - Y_r'^2}$.

To move from point B to the destination point C, the value of the reactance needs to be changed to zero. The magnitude of this move also can be estimated based on the value of reactance on the perfect-match resistance circle, at each conductance circle, i.e., for each $x = Y_r'$. We use the third-order polynomial

$$\Delta_{\text{mov2}} = 4.1 - 13.2x + 18.5x^2 - 9.4x^3 \tag{19}$$

to estimate the reactance at each conductance circle and, thus, the length of the second move.

The previous explanation can be applied to the left half of the Smith chart as well. Impedance and admittance will change place, and thus, the same polynomials could be used, given that this time, $x = Z_r'$, and $\Delta_{\text{mov1}} = |Z_i' - y|$.

The control unit adjusts the values of the bias voltages according to Δ_{mov1} and Δ_{mov2} and passes them to the matching unit, where the capacitance and inductance values are set following (10)–(13).

E. Flowchart Summary

Fig. 12 provides the flowchart of the proposed impedance-matching solution. It summarizes the details presented in the previous subsections and includes the steps from the time the system measures the access impedance up to the final circuit structure and parameter values, which are employed in the final matching circuit.

V. Simulation Results

The proposed impedance-matching system was modeled behaviorally, described in the Very high-speed integrated circuit Hardware Description Language-Analog and Mixed Signal (VHDL-AMS), and simulated in Cadence. Here, we first describe the access-impedance settings that we used for our experiments and then present and discuss simulation results. To gain insight into the performance of the matching circuit, three types of simulation results are presented: transmitter-side stand-alone matching, receiver-side stand-alone matching, and concurrent transmitter-side and receiver-side matching.

A. Test Parameters

The shaded area of the Smith chart in Fig. 13 shows the range of possible access impedances for the frequency range from 1 to 100 MHz that we have measured for two different vehicles [16], [21]. Since reference impedance is $Z_0 = 50\ \Omega$, the plotted range corresponds to impedances from $\approx 0\ \Omega$ to 250 Ω for the real part and $-175\ \Omega$ and $+150\ \Omega$ for the imaginary part, respectively. To evaluate the performance of the impedance matching under different scenarios, the access-impedance points shown in Fig. 13 have been selected for simulations.[2] Given the selected impedance values, the matching circuit has been simulated at different frequencies.

[2]We note that we do not have sufficient data to assign probabilities of occurrence to impedance values, and thus, it is not clear, at this point, what cases occur relatively more frequently or less. Hence, we have tried to select impedance values that are spread across a fairly wide range.

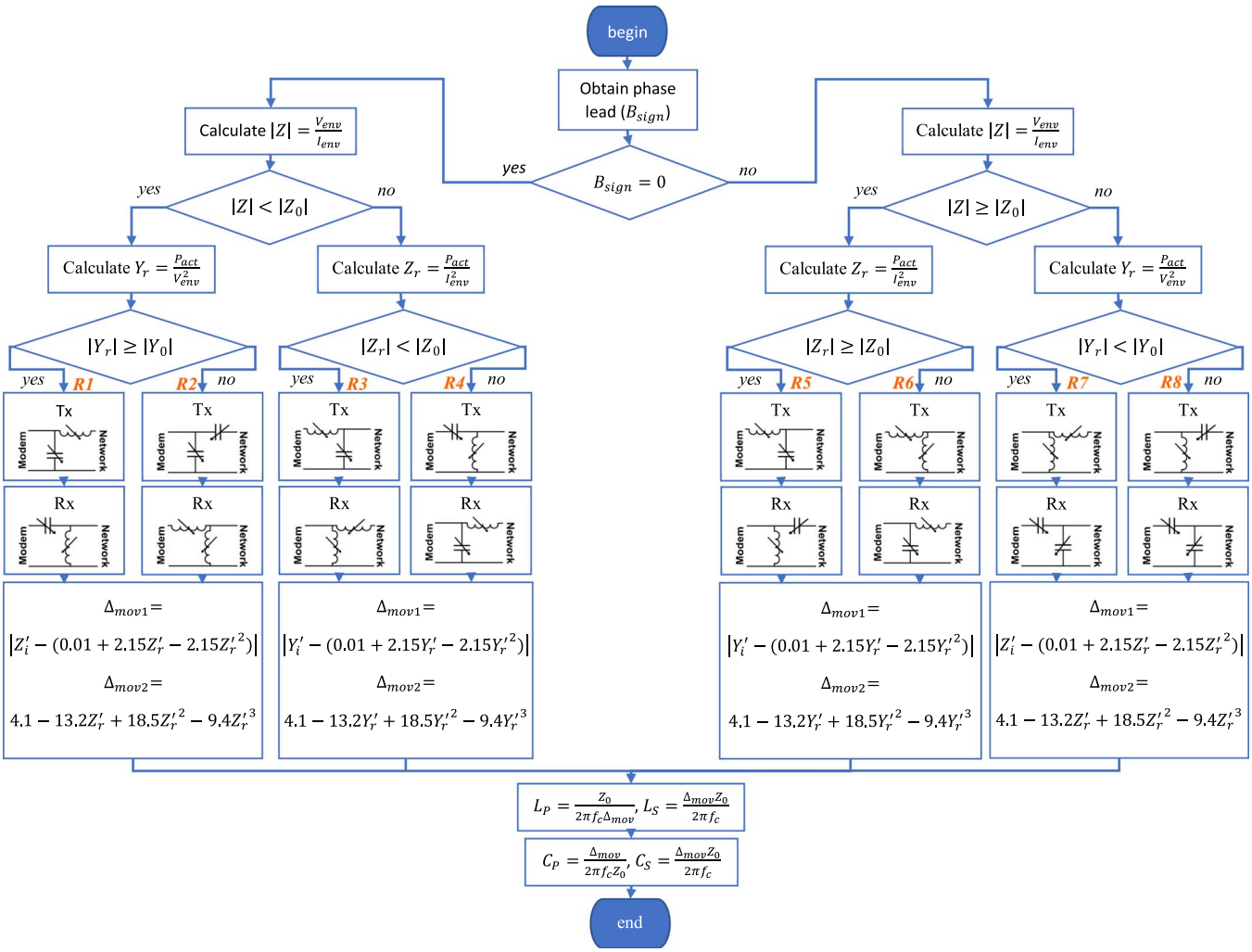

Fig. 12. Flowchart summary of the proposed adaptive impedance-matching technique, where "Ri" refers to the region i, which is identified in Fig. 3 and listed in Tables V and VI.

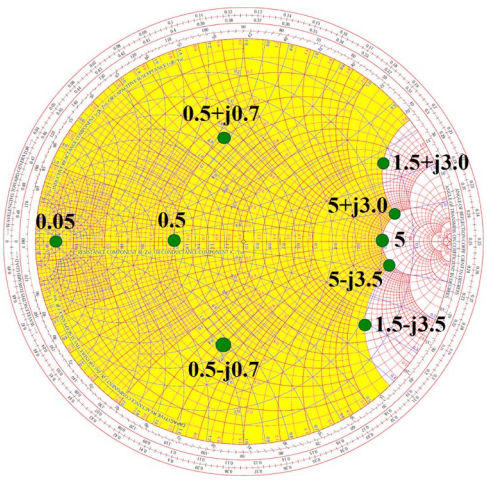

Fig. 13. Colored area shows the access-impedance range for VPLC applications for frequencies between 1 and 100 MHz [16], [21], and each dot represents a test point. The values on the chart are normalized to 50 Ω.

Furthermore, to evaluate the performance of the circuit when operated around the carrier frequency f_c, bandwidth simulations have been performed. For these tests, the impedance matching has been performed at frequency f_c, and then, with matching disabled, the signal frequency was altered around f_c to evaluate the bandwidth performance. Table VII lists the four center frequencies and frequency bands that have been tested and led to the results presented in Section V-C and D. For each of them, three access-impedance values were assumed, according to the maximum, one tenth of the maximum, and average impedance, as measured in [18], for the corresponding frequency f_c. To model the impedances for the entire tested band, we used passive elements (resistors and inductors) with fixed values. The real part of the impedances in Table VII gives the resistance values, and the inductances are the imaginary part divided by $2\pi f_c$.

TABLE VII
PARAMETERS FOR BANDWIDTH SIMULATIONS

f_c [MHz]	Tested band [MHz]	Access Impedance at f_c [Ω]		
		Maximum	Maximum/10	Average
10	7.5-12.5	$100 + j60$	$10 + j6$	$10 + j20$
30	25-35	$100 + j45$	$10 + j4.5$	$20 + j25$
50	40-60	$260 + j60$	$26 + j6$	$40 + j40$
80	65-95	$150 + j140$	$15 + j14$	$75 + j30$

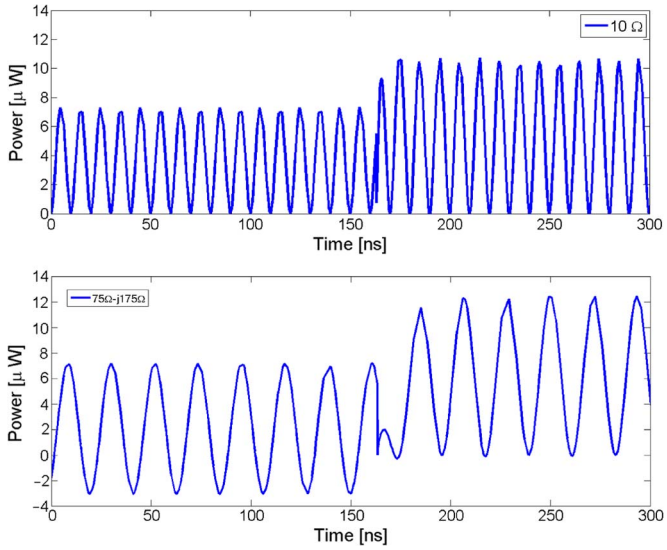

Fig. 14. Impedance matching, considering instantaneous power $P_s(t)$ from the source into the network with an access impedance of 10 Ω (top) and (75 − j175) Ω (bottom), respectively. Impedance matching is activated at $t = 150$ ns.

Finally, for simulations of concurrent transmitter-side and receiver-side matching in Section V-E, we use the S-parameters of the links measured in our campaigns [16], [21] to emulate the network characteristics.

B. Time-Domain Illustration of Matching

We first illustrate the effect of transmitter-side impedance matching by considering the instantaneous power signal $P_s(t)$ from (8) at the transmitter side. Fig. 14 shows $P_s(t)$ for an access impedance of 10 Ω and (75 − j175) Ω, respectively. The matching is activated at $t = 150$ ns. We observe that, after $t = 150$ ns, the adaptive impedance-matching system adjusts the matching circuit, such that it improves the power transfer from the source into the network. For the case of the 10-Ω access impedance (see the top graph in Fig. 14) both the power envelope, i.e., $V_{\rm env} I_{\rm env}$, and the phase term $\cos(\phi)$ have increased after matching; in the other case (see the bottom graph in Fig. 14), the active power is increased mostly due to better matching of the phase.

Fig. 15 illustrates the transmitter-side and receiver-side matching for a communication link, by showing the instantaneous and active signal power received by the receiver of the communication link. To model the link, we apply the S-parameters for the VCU-DC/DC link from [16] (see Table IV). As described in Section IV-A, the system uses a preamble signal to perform the matching. In this example, this is done in two stages. First, the transmitter sends the test signal and performs the matching at $t = 1$ μs. As we can observed in the left subplot of Fig. 15, the power transmitted to the receiver increases due to the larger power inserted into the network from the transmitter side. Then, the test signal is sent from the receiver side at $t = 2$ μs. In the middle subplot of Fig. 15, the power received at the receiver is negative since it is injecting power during this period. Note the different y-axis scale for this subplot, which is due to the signal measured before it undergoes channel attenuation. Matching is performed at $t = 3.2$ μs. Finally, the system goes into operation mode, where communication could be performed at $t = 4$ μs (right subplot). Overall, the power transfer from the transmitter to the receiver is tripled after both matching circuits have been adapted (after $t = 4$ μs) compared to the original state without matching (before $t = 1$ μs).

We note that the active power shown in Fig. 15 is $P_{\rm act}(t)$ in (9), as provided by the measurement unit. We observe that it takes about 0.5 μs for the measurement circuit to settle to its final value, which determines the time that is required for the matching process.

C. Transmitter-Side Matching

We now present results for transmitter-side matching, considering the access-impedance range discussed in Section V-A. The source impedance of the communication transmitter is set to 50 Ω.

Fig. 16 shows the normalized active power transmitted into the network with and without impedance matching, for different frequencies and access-impedance values. Normalization is with respect to the active power when optimal matching is applied, i.e., a normalized active power of one is the best possible performance. The top and bottom subfigures in Fig. 16 are for inductive and purely resistive access impedances, respectively. We observe that, for most access-impedance values, impedance matching significantly improves the active-power transfer and that this applies for sampled frequency values from a wide range. The exception is the very low-resistance case of 2.5 Ω, for which matching does not show an improvement. We attribute this to rapid changes of the values needed for compensation at the low-resistance end, which causes larger estimation errors from fitting susceptance and reactance changes [estimated by (17)–(19)]. We also note that a wrong estimation in the first move could itself lead to a degraded matching, regardless of the quality of the second move. For all other impedance cases, however, matching can improve the power transmission to about 70% and more of the ideally matched case.

Further insight into the performance of our impedance-matching solution is provided through Fig. 17, which shows the normalized active-power transfer as a function of the resistance of a purely resistive access impedance at a frequency of $f_c = 50$ MHz. We observe that impedance matching consistently improves performance, but the gap to the ideal matching increases drastically for access impedances below approximately 8 Ω. This could be improved by providing better estimation functions than (18) and (19), by, e.g., using a higher order polynomial expression. We also note that the dimension of the sensing resistor in the measurement unit is critical, particularly for access impedances with very low resistance. To avoid potential performance degradation because of distorted measurements, the sensing resistor had been chosen as 0.1 Ω.

Finally, in Fig. 18, we show the results of the bandwidth simulations, according to the parameters specified in Table VII. It can be observed that the matching system shows an overall fairly flat in-band behavior. Even when there is deviation from the matching frequency f_c, still significant improvements in signal-power transfer compared to transmission without

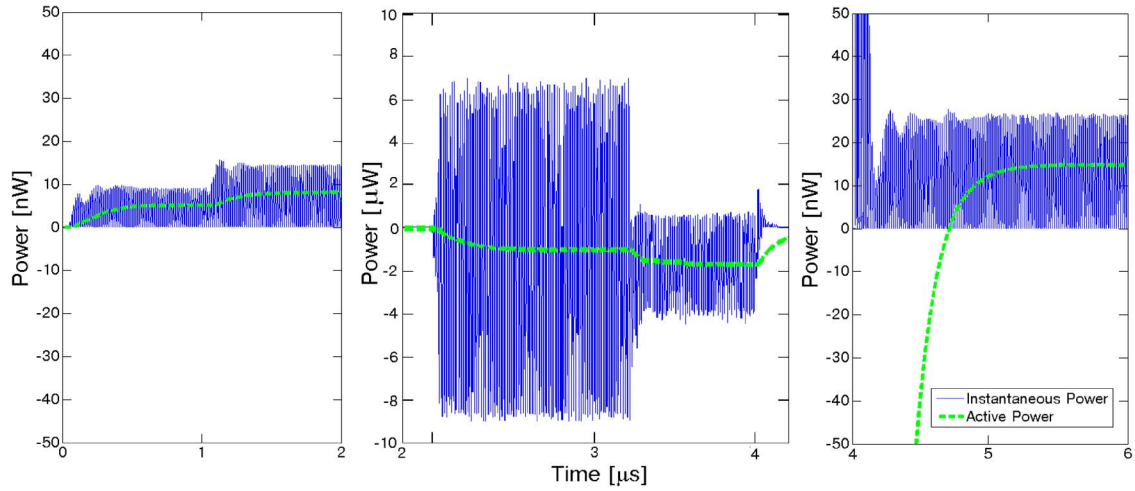

Fig. 15. Transmitter-side and receiver-side matching for VCU-DC/DC link. Curves are the power received at the receiver of the communication link. Transmitter performs matching at $t = 1$ μs (left subplot). Receiver sends a test signal at $t = 2$ μs to perform matching, which happens at $t = 3.2$ μs (middle subplot). Finally, at $t = 4$ μs, the system goes into data-transmission mode (right subplot).

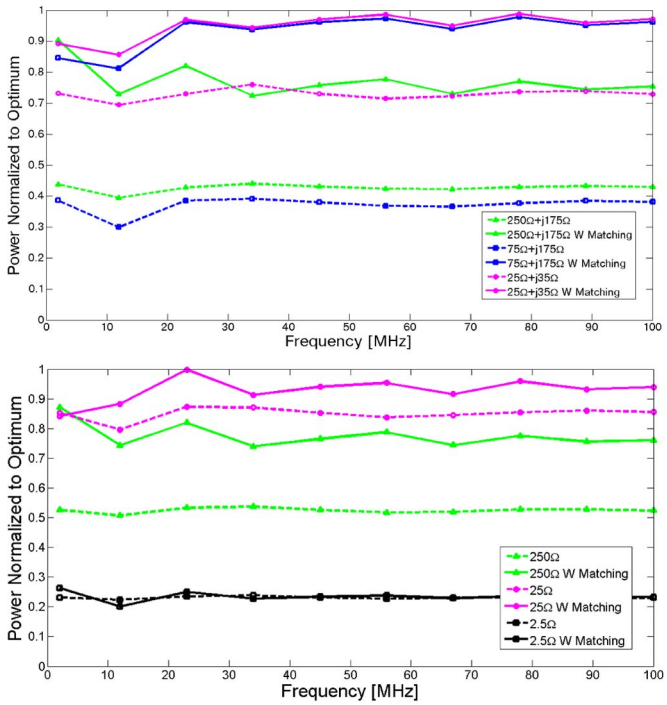

Fig. 16. Normalized active power transferred into the network as a function of frequency with (solid lines) and without (dashed lines) transmitter-side impedance matching for different access impedances. (Top) Inductive access impedance. (Bottom) Purely resistive access impedance.

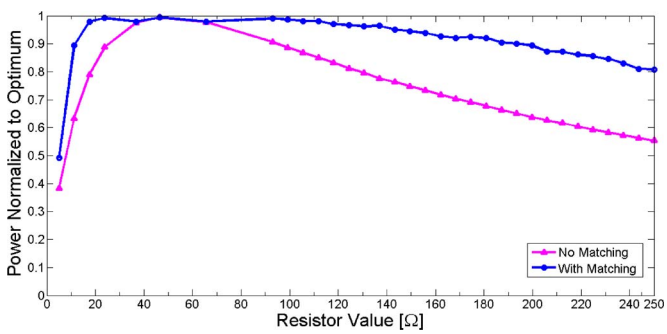

Fig. 17. Normalized active power transferred into the network as a function of resistance for purely resistive access impedance. Frequency $f_c = 50$ MHz.

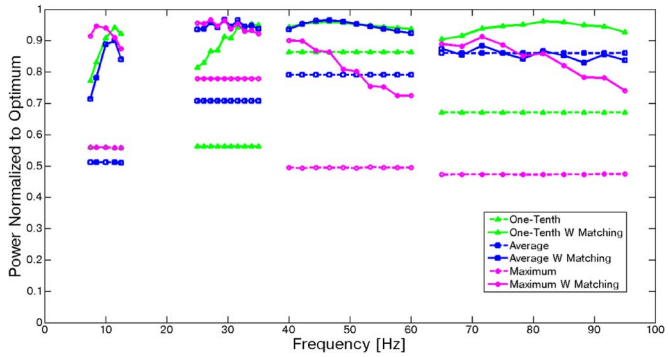

Fig. 18. Normalized active power transferred into the network as a function of frequency with (solid lines) and without (dashed lines) transmitter-side impedance matching. Bandwidth results of the impedance matching for the test cases specified in Table VII.

matching are achieved. In particular, active power transmitted into the network with matching is always within 30% of the ideal condition. Therefore, under such conditions, the matching circuit can be considered as wideband and used for a more broadband signal transmission once fixed and adjusted at a center frequency.

D. Receiver-Side Matching

The second set of results is for receiver-side matching. The impedance of the communication receiver is assumed to be 50 Ω.

Fig. 19 shows the performance, again in terms of normalized power transfer, here from the network into the communication receiver, as a function of frequency and for different capacitive access impedances (top subfigure) and as a function of the resistance of a purely resistive access impedance at $f_c = 50$ MHz (bottom subfigure). We observe that, in all cases, the amount of signal power extracted from the network is greatly improved and approaches that of the ideal matching within 30%. A notable similarity to the results from the previous section for transmitter-side matching is the degradation of the transferred power at low-resistance impedances for similar reasons.

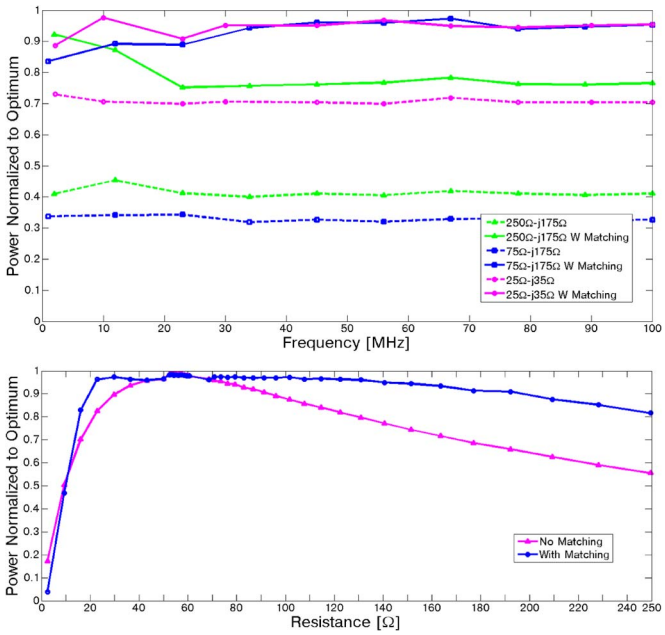

Fig. 19. Normalized active power extracted from the network with and without adaptive impedance matching at the receiver side. (Top) Different capacitive access-impedance results with (solid lines) and without (dashed lines) matching as a function of frequency. (Bottom) Performance as a function of resistance for a purely resistive access impedance and $f_c = 50$ MHz.

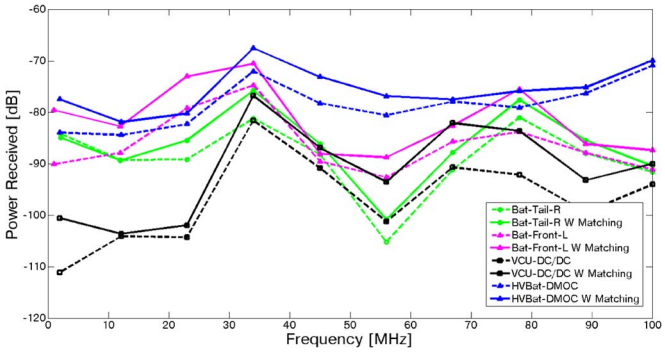

Fig. 20. Active power at the receiver as a function of frequency with (solid lines) and without (dashed lines) impedance matching for four different communication links. In all cases, transmitter is a voltage source with an amplitude of 50 mV, and both transmitter and receiver have a 50-Ω resistance.

E. Matching at Both Ends of the Communication Link

We now show the active-power transfer from the transmitter of the communication system to the receiver, when the proposed adaptive impedance matching is performed at both ends of the communication link. To evaluate the performance of the system under realistic circumstances of VPLC, the S-parameters obtained in our measurement campaigns [16], [21] were used to describe the network. Fig. 20 shows the receiver's active power for transmission with and without matching for four links as a function of frequency. We note that the fluctuation of curves with frequency is due to the frequency-dependent channel attenuation, which affects the measured received power. Comparing the results for with and without matching, we observe improvements in the received power between 1 and 10 dB.

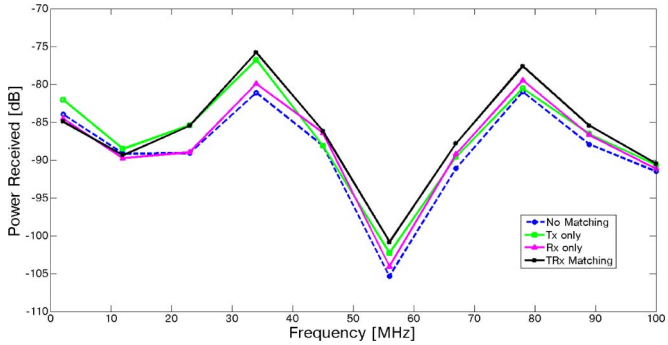

Fig. 21. Active power at the receiver as a function of frequency with (solid lines) and without (dashed lines) impedance matching for the Bat-Tail-R link. Transmitter-side matching ("Tx only"), receiver-side matching ("Rx-only"), and concurrent transmitter- and receiver-side matching ("TRx Matching") are considered. In all cases, transmitter is a voltage source with an amplitude of 50 mV, and both transmitter and receiver have 50-Ω resistance.

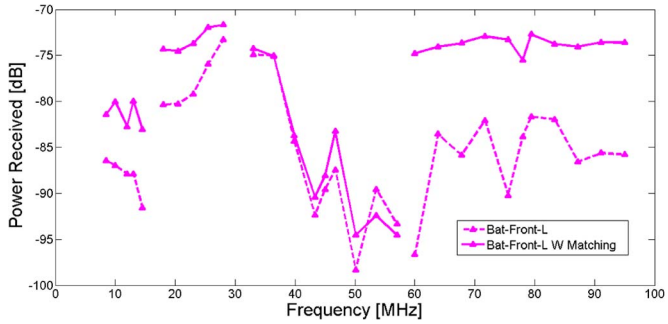

Fig. 22. Active power transferred from transmitter to receiver as a function of frequency with (solid lines) and without (dashed lines) impedance matching for the Bat-Tail-L link. For this bandwidth results, matching is adjusted at the frequency points $f_c = \{12, 23, 45, 78\}$ MHz. In all cases, the transmitter is a voltage source with an amplitude of 50 mV, and both transmitter and receiver have 50-Ω resistance.

In other words, up to about ten times more signal power arrives at the receiver due to matching.

To further investigate the distinct effect of matching at each end of the link, Fig. 21 shows the received active power for the cases of no matching, only transmitter-side matching, only receiver-side matching, and concurrent transmitter-side and receiver-side matching, for one of the links in Fig. 20 (i.e., the Bat-Tail-R link [21]). We observe that, for most frequency values, the concurrent matching offers the best performance. The contributions from matching at each end of the link is frequency dependent, which is due to the different S-parameters and, thus, different access impedances for different frequencies. Furthermore, in a few instances, we note that only transmitter-side matching would result in somewhat higher received power than matching at both ends. In these cases, another adjustment of the matching circuit at the transmitter, after adjustment of the receiver-side matching, would be beneficial.

Finally, the results for bandwidth simulations are shown in Fig. 22. Here, we selected the Bat-Front-L link in [21] also considered in Fig. 20. Matching is done for the frequency points $f_c = \{12, 23, 45, 78\}$ MHz and tested in a bandwidth of about $0.2f_c$ around the f_c value. It can be observed that, in most cases, the matching adjusted at the center frequency leads to

TABLE VIII
COMPARISON OF CURRENT WORK WITH RELATED WORKS

Work	[27]	[20]	[28]	[29]	This work
Methodology	Analytical	Analytical	Numerical	Analytical	Analytical
Impedance Type	Insertion Loss	Single	Single	Single	Single
Structure	Fixed	Fixed	Flexible	Flexible	Flexible
Implementation	Passive	Combination	Passive	Combination	Combination
Bandwidth	Narrow	Narrow	Wide	Narrow	Narrow/Wide
Frequency (MHz)	13.56	0.132	[1.5-22]	5.5	[1-100]
Impedance (Ω)	[1-100]	[3-10] + j[0.0008-0.83]	[0-400] $\angle$[0-$\pm$75]	[0.32-25.2] + j[5.97-9.3]	[2.5-250] + j[$\pm$4.5-$\pm$175]
Maximum Power Improvement Ratio	N/A	N/A	3.6	7.6	10

an improved power transmission over a wider range around the center frequency. Only for the case of adjusting the matching at $f_c = 45$ MHz and operating at above 55 MHz, we note a loss in received power due to matching mismatch. We also observe that changes in the power transmission over frequency are often smoother and/or better bounded after matching has been applied. Hence, the proposed matching also improves relatively broadband transmission.

F. Comparison

To put the features and results of the suggested design into perspective, we have compared it with the related work discussed in Section II-B. In Table VIII, we observe that the proposed design achieves the largest maximum power gain (ratio of the power transfer after matching to that of before matching). Our solution is also tested and proven effective under the widest range of frequencies and loads, with the exception of [28], where a wider range of impedance has been compensated for. However, their maximum achievable power gain is considerably lower than that of the proposed work. Different from [28], which applies an M-PSO algorithm for parameter adjustment, our solution is based on closed-form expressions presented in Section IV, which results in significantly lower computational load. On the other hand, the approach in [28] applies to a wideband matching, whereas we target narrow-band matching. Our results have shown that the proposed system can be used for a relatively wider band around the center frequency. Being applicable to a wider band around the center frequency is an advantage compared to other narrow-band works listed in Table VIII.

VI. CONCLUSION

PLC over the automotive power harness would benefit from impedance matching at the transmitter and the receiver. More specifically, due to the variation of the channel over location and time, adaptive impedance matching is required. In this paper, we have presented a design approach for such an adaptive impedance-matching system. It includes the actual matching circuitry and a sensing measurement and a control unit to adjust the circuit components. The details of the design were presented, which were followed by demonstrations of the system performance using simulations for realistic test scenarios. Our numerical results demonstrated that, under a wide range of conditions, the proposed design achieves signal-power transfer close to that of optimal matching. Overall, power transfer gains achieved due to matching can be up to about 10 dB, which is larger than what has been reported in previous works in the literature. Furthermore, although our design is for narrow-band transmission, it often also improves the performance for broadband transmission around the nominal matching frequency.

ACKNOWLEDGMENT

The authors would like to thank CMC Microsystems for facilitating the CAD tool support and access to technology.

REFERENCES

[1] N. Taherinejad, R. Rosales, L. Lampe, and S. Mirabbasi, "On the design of impedance matching circuits for vehicular power line communication systems," in *Proc. IEEE ISPLC*, 2012, pp. 322–327.
[2] N. Taherinejad, L. Lampe, and S. Mirabbasi, "Adaptive impedance matching for vehicular power line communication systems," in *Proc. IEEE ISPLC*, Mar. 2014, pp. 214–219.
[3] M. Schwartz, "Carrier-wave telephony over power lines: Early history [history of communications]," *IEEE Commun. Mag.*, vol. 47, no. 1, pp. 14–18, Jan. 2009.
[4] H. Ferreira, L. Lampe, J. Newbury, and T. Swart, *Power Line Communications: Theory and Applications for Narrowband and Broadband Communications over Power Lines*. New York, NY, USA: Wiley, 2010.
[5] S. Galli, A. Scaglione, and K. Dostert, "Broadband is power: Internet access through the power line network," *IEEE Commun. Mag.*, vol. 41, no. 5, pp. 82–83, May 2003.
[6] G. Leen and D. Heffernan, "Expanding automotive electronic systems," *Computer*, vol. 35, no. 1, pp. 88–93, Jan. 2002.
[7] N. Navet, Y. Song, F. Simonot-Lion, and C. Wilwert, "Trends in automotive communication systems," in *Proc. IEEE*, vol. 93, no. 6, pp. 1204–1223, Jun. 2005.
[8] "Automotive multiplexing protocols: Cost/performance driving new protocol adoption," Strategy Anal. Newton, MA, USA, Autom. Electron. Rep., Nov. 2007, Accessed Aug. 28, 2011. [Online]. Available: http://www.businesswire.com/news/home/20071115006121/en/STRATEGY-ANALYTICS-Automotive-Electronics-Network-Market-Stretch
[9] P. A. J. van Rensburg and H. C. Ferreira, "Automotive power-line communications: favorable topology for future automotive electronic trends," in *Proc. IEEE ISPLC*, Kyoto, Japan, Mar. 2003, pp. 103–108.
[10] T. Enders and J. Schirmer, "Automotive powerline communications—A new physical layer for CAN," in *Proc. Int. CAN Conf.*, Munich, Germany, Oct. 2003, pp. 14–16.
[11] T. Huck, J. Schirmer, T. Hogenmuller, and K. Dostert, "Tutorial about the implementation of a vehicular high speed communication system," in *Proc. IEEE ISPLC*, Vancouver, BC, Canada, Apr. 2005, pp. 162–166.
[12] W. Gouret, F. Nouvel, and G. El-Zein, "Powerline communication on automotive network," in *Proc. IEEE VTC–Spring*, Apr. 2007, pp. 2545–2549.
[13] O. Amrani and A. Rubin, "Contention detection and resolution for multiple-access power-line communications," *IEEE Trans. Veh. Technol.*, vol. 56, no. 6, pp. 3879–3887, Nov. 2007.
[14] M. Lienard, M. O. Carrion, V. Degardin, and P. Degauque, "Modeling and analysis of in-vehicle power line communication channels," *IEEE Trans. Veh. Technol.*, vol. 57, no. 2, pp. 670–679, Mar. 2008.
[15] F. Benzi, T. Facchinetti, T. Nolte, and L. Almeida, "Towards the power-line alternative in automotive applications," in *Proc. IEEE Int. Workshop Factory Commun. Syst.*, May 2008, pp. 259–262.

[16] M. Mohammadi *et al.*, "Measurement study and transmission for in-vehicle power line communication," in *Proc. IEEE ISPLC*, Dresden, Germany, Mar./Apr. 2009, pp. 73–78.
[17] A. Vallejo-Mora, J. Sánchez-Martínez, F. Cañete, J. Cortés, and L. Díez, "Characterization and evaluation of in-vehicle power line channels," in *Proc. IEEE GLOBECOM*, Dec. 2010, pp. 1–5.
[18] N. Taherinejad, R. Rosales, L. Lampe, and S. Mirabbasi, "Channel characterization for power line communication in a hybrid electric vehicle," in *Proc. IEEE ISPLC*, 2012, pp. 328–333.
[19] S. Barmada, M. Raugi, M. Tucci, Y. Maryanka, and O. Amrani, "PLC systems for electric vehicles and smart grid applications," in *Proc. IEEE ISPLC*, Johannesburg, South Africa, Mar. 2013, pp. 23–28.
[20] M. Antoniali, M. De Piante, and A. M. Tonello, "PLC noise and channel characterization in a compact electrical car," in *Proc. IEEE ISPLC*, Johannesburg, South Africa, Mar. 2013, pp. 29–34.
[21] V. Degardin, M. Lienard, P. Degauque, E. Simon, and P. Laly, "Impulsive noise characterization of in-vehicle power line," *IEEE Trans. Energy Convers.*, vol. 50, no. 4, pp. 861–868, Nov. 2008.
[22] C.-Y. Park, K.-H. Jung, and W.-H. Choi, "Coupling circuitary for impedance adaptation in power line communications using VCGIC," in *Proc. IEEE ISPLC*, Jeju, South Korea, Apr. 2008, pp. 293–298.
[23] N. Taherinejad, R. Rosales, S. Mirabbasi, and L. Lampe, "A study on access impedance for vehicular power line communications," in *Proc. IEEE ISPLC*, Udine, Italy, Apr. 2011, pp. 440–445.
[24] V. Iyer and S. Makarov, "A lumped circuit for wideband impedance matching of a non-resonant, short dipole or monopole antenna," in *Proc. IEEE APSURSI*, Jun. 2009, pp. 1–4.
[25] D. Pozar, *Microwave Engineering*. New Delhi, India: Wiley-India, 2009.
[26] B. Yarman, M. Şengül, J. Trabert, K. Blau, and M. Hein, "Design of wideband matching networks for wireless communication systems," in *Proc. Int. Symp. Commun. Control Signal Process.*, Mar. 2006, pp. 1–4.
[27] B. Godara and A. Fabre, "Versatile wideband impedance matching circuit based on current conveyors," *Electron. Lett.*, vol. 43, no. 6, pp. 37–38, Mar. 2007.
[28] H. Carlin and J. Komiak, "A new method of broad-band equalization applied to microwave amplifiers," *IEEE Tran. Microw. Theory Techn.*, vol. MTT-27, no. 2, pp. 93–99, Feb. 1979.
[29] A. Mavretic, A. Ciszek, and J. Stach, "Apparatus for Matching a Variable Load Impedance With an RF Power Generator Impedance, US Patent 5,654,679, Aug. 5, 1997.
[30] R. Araneo, S. Celozzi, and G. Lovat, "Design of impedance matching couplers for power line communications," in *Proc. IEEE Int. Symp. EMC*, Aug. 2009, pp. 64–69.
[31] P. Nisbet, M. He, and L. Zhao, "Transformerless impedance matching networks for automotive power line communication," *J. Electr. Electron. Eng. Res.*, vol. 6, no. 2, pp. 13–20, Aug. 2014.
[32] A. Leuciuc and L. Goras, "New general immittance converter JFET voltage-controlled impedances and their applications to controlled biquads synthesis," *IEEE Trans. Circuits Syst. I, Fundam. Theory Appl.*, vol. 45, no. 6, pp. 678–682, Jun. 1998.
[33] "Low-Noise Amplifier Stability Concept to Practical Considerations, Part 2," Maxim Integr., San Jose, CA, USA, Oct. 2014. [Online]. Available: http://www.maximintegrated.com/en/app-notes/index.mvp/id/1851

Nima Taherinejad (S'08–M'15) received the B.Sc. degree in electrical and electronic engineering from the Babol Noshirvani University of Technology, Babol, Iran, in 2007; the M.Sc. degree in electrical and electronic engineering from the Iran University of Science and Technology, Tehran, Iran, in 2009; and the Ph.D. degree in electrical and computer engineering from The University of British Columbia, Vancouver, BC, Canada, in 2015.

He is currently a Postdoctorate University Assistant with the TU Wien (formerly known also as Vienna University of Technology), Vienna, Austria, where his main areas of research include systems on chip, self-awareness in cyberphysical systems, embedded systems, and robotics. He has authored a book and published in/served as a reviewer for various journals and conferences.

Dr. Taherinejad has received several awards and scholarships from universities and conferences he has attended.

Lutz Lampe (M'02–SM'08) received the Dipl.-Ing. and Dr.-Ing. degrees in electrical engineering from the University of Erlangen, Erlangen, Germany, in 1998 and 2002, respectively.

Since 2003, he has been with the Department of Electrical and Computer Engineering, The University of British Columbia, Vancouver, BC, Canada, where he is a Full Professor. His research interests are broadly in theory and application of wireless, optical wireless, power line, and underwater acoustic communications.

Dr. Lampe is currently an Associate Editor of the IEEE WIRELESS COMMUNICATIONS LETTERS and the IEEE COMMUNICATIONS SURVEYS AND TUTORIALS, and he has served as an Associate Editor and a Guest Editor of several IEEE transactions and journals. He was a (co)recipient of a number of Best Paper Awards, including awards at the 2006 IEEE International Conference on Ultra-Wideband, the 2010 IEEE International Communications Conference, and the 2011 IEEE International Conference on Power Line Communications. He is a Coeditor of the book *Power Line Communications: Principles, Standards and Applications from Multimedia to Smart Grid (2nd ed.)* (Wiley).

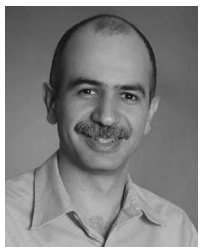

Shahriar Mirabbasi (S'95–M'02) received the B.Sc. degree in electrical engineering from Sharif University of Technology, Tehran, Iran, in 1990 and the M.A.Sc. and Ph.D. degrees in electrical and computer engineering from the University of Toronto, Toronto, ON, Canada, in 1997 and 2002, respectively.

Since August 2002, he has been with the Department of Electrical and Computer Engineering, The University of British Columbia, Vancouver, BC, Canada, where he is currently a Professor. His current research interests include analog, mixed-signal, radio frequency (RF), and millimeter-wave integrated circuit and system design with particular emphasis on wireless and wireline communications, silicon photonics, RFID, sensor interface, and biomedical applications.